

Emission-Line Properties of 3CR Radio Galaxies III: Origins and Implications of the Velocity Fields

Stefi A. Baum¹ & Patrick J. McCarthy^{2,3}

Received _____; accepted _____

¹The Space Telescope Science Institute,
3700 San Martin Dr., Baltimore, MD 21218

²The Observatories of the Carnegie Institution of Washington,
813 Santa Barbara St., Pasadena, CA 91101

³Guest Observer at the National Optical Astronomy Observatories, Cerro Tololo
Interamerican Observatory, which is operated by the Associated Universities for Research in
Astronomy, Inc., under contract with the National Science Foundation

ABSTRACT

We present the results of an analysis of the large scale velocity fields of the ionized gas associated with powerful radio galaxies. Long-slit spectra of 52 objects provide a sample of resolved velocities that span a wide range of redshifts, radio and emission-line luminosities. Line widths reaching 1000 km s^{-1} and resolved velocity fields with amplitudes of up 1500 km s^{-1} are found on scales from 10 to 100 kpc in the environments of radio galaxies at redshifts larger than 0.5. The global velocities and FWHM are of comparable amplitudes in the FRII sources, while the FRI sources have FWHM values that are larger than their resolved velocity fields. We find evidence for systematically larger line widths and velocity field amplitudes at $z > 0.6$. Several of the largest amplitude systems contain two galaxies with small projected separations. All of the $> 1000 \text{ km s}^{-1}$ systems occur in objects at $z > 0.6$ and all have comparable radio and [OII] sizes. There is a weak correlation of off-nuclear line widths and velocity field with the ratio of the radio and emission-line sizes, but it is of low statistical significance and there is a very large dispersion. The change in properties at redshifts above $z \sim 0.6$ could reflect a difference in environments of the host galaxies, with the hosts inhabiting higher density regions with increasing redshift (e.g., Hill & Lilly 1991). The mass of ionized gas and the apparent enclosed dynamical mass are correlated and both increase steeply with redshift and/or radio power.

The origin of the velocities remains uncertain. The data do not require jet-gas interactions to explain the kinematics and superficially are slightly more consistent with gravitational origins for the bulk of the kinematics. If the line width reflects the underlying gravitational potential, the observed FWHM traces the velocity dispersion of the host galaxy or its surrounding group or cluster. The highest velocities seen then point to interesting environments for intermediate and high redshift radio galaxies. Turbulent interactions with the expanding radio source as the origin of the kinematics are certainly not ruled out. In the jet interaction scenario, the maximum velocities seen in the nebula can be used to constrain the density of the pre-shock gas to be roughly $n_e > 0.6 \text{ cm}^{-3}$.

1. Introduction

We report the results of an investigation of the kinematic, ionization and morphological properties of the emission-line nebulae in powerful radio galaxies. We have analyzed long slit optical spectroscopic and narrow band imaging observations of large samples of low (Baum, Heckman, and van Breugel 1990). Tadhunter, Fosbury, & Quinn 1989) and intermediate to high redshift radio galaxies (McCarthy, Spinrad & van Breugel 1995; McCarthy, Baum, and Spinrad 1996). We utilize radio data from the literature. The combined data allow us to address questions concerning as the nature and origin of the emission line gas, the source of energy for the kinematic behavior of the gas, the relationship of the gas and radio activity to the host galaxy, and the nature of changes in gaseous environment or host properties as a function of epoch, environment, radio power and source structure.

Previous such studies have focused primarily on narrow redshift ranges or specific source types (e.g., Baum, Heckman & van Breugel 1992; Tadhunter et al. 1989, Gelderman & Whittle 1994; Villar-Martin et al. 1998). The sample amassed here allows us to address the relevant issues over a much wider range of radio luminosity and redshift. In particular, with this sample, we examine changes in the properties of the nebulae and their relationship to the radio source and host galaxy over the range of redshifts where we currently believe that both the host galaxies of powerful radio sources and their environments are evolving rapidly, $0.3 < z < 2$. Similarly, we examine the evidence for increased interaction between the radio source and its gaseous environment as a function of extended radio power and redshift.

In the low redshift sample considered by Baum, Heckman, & van Breugel (1992), they concluded that the bulk of the emission line gas kinematics were dominated by gravitational motions. For that sample it proved straightforward to statistically separate gas kinematics attributable to radio jet-gas interactions from those determined by the underlying gravitational potential of the host galaxy. If we are able to perform a similar separation at higher redshift, then we could use the gas kinematics as a function of redshift as a tracer of the evolution of the gravitational potential of the underlying host galaxies (the bright ellipticals) and their environments. Conversely, if we can show that the gas kinematics either in individual sources or overall, are due to interactions with the out-flowing radio jets, then carefully follow-up studies of individual sources should lead to a better understanding of jet physics (e.g., Clark et al. 1998). Lastly, the apparent increase in the number of close companion galaxies and possible clusters at $z > 0.5$ (e.g. Hill & Lilly 1991; Yates et al. 1989; Ellingson, Green, & Yee 1991) offer the possibility that kinematics of the emission-line gas may probe tidal interactions and cluster potentials on 100 kpc scales.

The 3CR and 1Jy class sources that we consider here comprise a representative sample of the most luminous radio sources at all redshifts less than 3. At redshifts greater than ~ 0.1 , they are primarily of the double-lobed Fanaroff & Riley (1974) type II morphologies and have luminosities that range from $10^{42} - 10^{45}$ erg sec $^{-1}$. The emission-line regions are seen on scales of up to 300 kpc and arise from low density gas in moderate to high ionization levels. The luminosities of the emission-line regions range from $10^{41} - 10^{44}$ erg sec $^{-1}$ and scale roughly with the radio luminosity (e.g. Rawlings and Saunders 1991; Baum, Heckman and van Breugel 1989a,b; McCarthy 1993; Xu, Livio, and Baum 1999). The total mass of ionized gas is uncertain but reasonable estimates range up to a few $\times 10^8 M_{\odot}$. The source of the ionization is also uncertain and is probably a mix of collisional heating and photo-ionization, with nuclear photo-ionization likely dominating the total line luminosities over a large range of radio power and redshift (e.g. Robinson et al. 1987; Baum and Heckman 1989a,b; Rawlings and Saunders 1991; Baum, Zirbel, and O'Dea 1995; Villar-Martin et al. 1997, Tadhunter et al. 1998). The general alignment of the emission-line regions with the axes defined by the radio lobes in nearly all powerful Fanaroff and Riley Class II type radio galaxies (e.g. Baum & Heckman 1989a,b; McCarthy et al. 1987; de Vries et al. 1999) is taken as further support for the presence of central photo-ionization by an anisotropic UV source. The precise spatial coincidence between radio hot-spots and jets with bright emission-line regions in some sources (e.g. de Vries et al. 1999; Miley et al. 1992, Villar-Martin et al. 1998), and the correlation between lobe and emission-line asymmetries (McCarthy, van Breugel, & Kapahi 1991) argues that shock heating is also an important process (e.g. Bicknell & Koekemoer 1995; Best et al. 1999).

In section 2, we describe the definition of the sample, the origin of the data, and the derived quantities which are used in the analysis. In section 3, we describe the results of the statistical analysis of the derived quantities. In section 4, we describe the correlation results. In section 5, we discuss the implications of these results and finally in section 6 we summarize the results and their implications.

1.1. The sample

The majority of the objects are drawn from the 3CR sample (Bennet 1962; Spinrad et al. 1985, Djorgovksi et al. 1988; Strom et al. 1990). At redshifts larger than ~ 0.2 nearly all of the 3CR galaxies that are known to have emission lines with extents of more than 5" are included in our sample. The source samples in Baum, Heckman, & van Breugel (1990, 1992) & McCarthy, Baum, & Spinrad (1996) were drawn from the emission-line

imaging surveys of a 408 MHz radio flux limited sample of low redshift equatorial radio sources by Baum et al. (1988) and a sample of intermediate and high redshift 3CR galaxies imaged by McCarthy et al. (1995). The latter sample becomes significantly incomplete for $1.2 < z < 1.6$, where the principal lines that show large spatial extents (e.g. [OIII]5007, [OII]3727, Ly α) are either unreachable or are in regions of very strong sky emission. In the range $0.2 < z < 1.2$ our sample contains all of the 3CR galaxies with large emission-line regions except 3CR 172, 3CR 275, 3CR 341, 3CR 244.1, 3CR 284, 3CR 180. At larger redshifts we do not have adequate 2-D spectra of the extended gas in 3C 437 ($z = 1.48$), 3C 256 ($z = 1.82$), 3C 326.1 ($z = 1.82$), 3C 454.1 ($z = 1.84$), and 3C 257 ($z = 2.4$). We have excluded the two Virgo sources (3C 272.1 & 3C 274) from our analysis as their linear extents are smaller than the resolution element for nearly all of the other objects in the sample. In addition to the 3CR sources, at low redshift our sample includes three Parkes sources (PKS 0634-206, PKS 0745-191, and PKS 1345+125) from the equatorial sample of Baum et al. (1988). Similarly, at $z > 2$ we have added three sources from the 408MHz MRC/1Jy survey (McCarthy et al. 1996). These three objects are thought to be representative of the large Ly α emission regions in the most distant radio galaxies.

2. The Data

We use ground-based long slit spectra and emission line images of 3CR and 1 Jy class radio galaxies that were obtained at the Kitt Peak and Cerro Tololo National Observatories, Lick Observatory, and Palomar Observatory. The details of the observations and the basic data are presented in Baum, Heckman, and van Breugel (1990), McCarthy, Spinrad and van Breugel (1995) and references therein. To this data we added similar data from the literature (e.g. Heckman *et al.* 1989; Tadhunter *et al.* 1989; Clark *et al.* 1998) as well as published radio maps (notably the compilation by Leahy, Bridle, & Strom (1996) of radio source maps for the 3CR) to assemble the data used to derive the correlations presented here.

2.1. Measured quantities

- FWHM - For each velocity field plotted in either Baum, Heckman, & van Breugel (1990) or McCarthy, Baum, & Spinrad (1995) we determined a characteristic

extra-nuclear FWHM. We used the maximum value of the FWHM, excluding both the nucleus and the regions where the uncertainties are large. We averaged over three spatial resolution elements at the location of the maximum FWHM in assigning a characteristic velocity width to the rather low signal-to-noise plots of FWHM vs. distance that are available for these objects. The tabulated values for the FWHM and our estimate of the associated uncertainties are given in columns 11 of Table 1.

The non-zero size of the spatial resolution elements in each spectra introduce a component of broadening to the lines that is not physical in origin. This is likely to be important in a number cases for which there are large velocity gradients (e.g. 3C 330) and for objects at high redshift where the spatial resolution element ($\sim 1.5''$) corresponds to scales of ~ 10 kpc.

- V_{peak} and V_{max} . We determined the maximum peak-to-peak amplitude of the resolved velocity field (V_{peak}) for each slit position and object combination. As with all of the measurements we averaged over a few spatial resolution elements and gave low weight to regions of the slit with large velocity uncertainties. Since many of the emission-line regions are distributed asymmetrically with respect to the nucleus, the peak-to-peak amplitude is often poorly defined. For this reason we define V_{max} - the maximum one-sided velocity offset with respect to the nucleus, regardless of its spatial location. Thus objects with large amplitude velocity fields, but one-sided nebulae (e.g. 3C 356) are properly compared with smaller amplitude, but symmetric, objects (e.g. 3C 300). Several of the objects were observed with more than one telescope and instrument combination, or in more than one position angle. For these we determined single values for the V_{peak} and V_{max} velocity amplitudes by choosing the data set with the highest resolution and signal to noise ratios. For objects with multiple position angles we use the angle that revealed the large velocities and line widths. In the cases of 3C 458 and 3C 265 for which two spatially offset slit positions were used, we included separate measurements for each. V_{peak} and V_{max} are tabulated in columns 6 & 7 of Table 1.
- $R_{V_{\text{max}}}$ and $D_{[\text{OII}]}$. Several of the derived quantities depend on both the observed velocities, or line widths, and a characteristic linear scale. We considered a number of different choices for this scale length and adopted two. The first is the isophotal size of the emission line region in kpc (denoted $D_{[\text{OII}]}$ in column 8 of Table 1) as determined from emission-line images (Baum et al. 1988; McCarthy, Spinrad and van Breugel 1995). These were measured at a fixed rest-frame surface brightness level corresponding to $f(\text{H}\alpha) = 3.0 \times 10^{-15} \text{ erg sec}^{-1} \text{ cm}^{-2}$ per square arcsecond. Images in [OIII], [OII] or Ly α were converted to equivalent H α surface brightnesses (McCarthy et al. 1995). The depth reached by the slit spectra and the narrow-band imaging

were not always identical, particularly when considering that not all of the region of detected emission in the spectra were of sufficient quality to allow for accurate velocity measurements. We also measured the distance from the nucleus to the point of maximum velocity directly from the spectra. This distance, $R_{V\max}$ is listed in column 9 in Table 1 and is used in several of the plots and computations.

- Radio source sizes, D_{Rad} and l_{Rad} - The linear (lobe separation) sizes of the radio sources are given as D_{rad} in Column 12 of Table 1. The angular sizes were either measured directly from the maps in Baum et al. (1988) or taken from the compilation in McCarthy, van Breugel and Kapahi (1991), and were then converted to kpc using $H_0 = 50 \text{ km sec}^{-1} \text{ Mpc}^{-1}$ and $q_0 = 0.1$. As discussed above, the emission-line regions are often one sided and a simple comparison between the maximum size of the radio source and emission-line region may not give a proper reflection of the degree of spatial coincidence between the radio and line-emitting material. We used the most recent maps to determine the angular size of the radio sources on the same side of the nucleus as the gas whose velocity field we measure. Thus for sources with asymmetric emission-line regions we tabulate the length of one arm of the radio source, while for more symmetric nebulae we tabulate the total size of the source. This emission-nebula dependent measure of the radio source extent is given as l_{rad} in Column 13 of Table 1. Sources with one sided nebulae and close coincidences between radio lobes and emission line regions (e.g. 3C 441) can now be recognized by the rough equalities of the two sizes in columns 8 and 13, in Table 1.

2.2. Derived quantities

- Gas mass, M_{gas} (column 14, Table 1). We estimated the total mass of line-emitting gas for each object in our sample. The masses were derived from the measured luminosities and characteristic scales determined from the emission-line images, and an assumed value of the ionization parameter of 1%. The filling factor, in units of 10^{-5} , is given by, $f_{v5} = 41.3 \times (U_{-2} \times r_{10}/L_{44})^{0.5}$, where U_{-2} is the ionization parameter in units of 10^{-2} , $U = Q(\text{ion})/4\pi r^2 n_e c$. The mass of gas, in units of $10^8 M_{\odot}$, is $1.4 \times (L_{44} \times r_{10}^3 \times f_{v5})^{0.5}$, where L_{44} is the equivalent [OII]3727 luminosity in units of 10^{44} erg/sec and r_{10} is the size of the emission-line nebulae in units of 10 kpc. These masses are highly uncertain as they, 1) make very simplified assumptions about the geometry of the line-emitting gas (a sphere of radius r_{10}), 2) adopt the same value of U_{-2} for all of the sources and 3) make no correction for ionization fraction, abundances etc.

- Dynamical Mass, M_{dyn} (column 17, Table 1). To the extent that the large scale velocity fields reflect the gravitational potential and are representative of the circular velocity, they can be used to infer an interior dynamical mass. We use the distance to the peak emission-line velocity, R_{Vmax} and the maximum velocity to compute the inferred enclosed mass in units of $10^8 M_{\odot}$ as $0.0022 \times R_{Vmax} \times V_{max}^2$ with R_{Vmax} in kpc and V in km/sec. This apparent or inferred dynamical mass only really measures mass if the kinematics are dominated by rotation in response to the gravitational field, and will have an entirely different meaning if the gas kinematics are set via radio source - cloud interactions.

3. Results

Our sample and the derived data are listed in Table 1. For each source we list a single set of measurements corresponding to the slit position angle with the largest velocities. For 3C 458 and 3C 265 we list two sets of measurements as they were taken at two different slit positions, one centered on the nucleus and a parallel slit position offset from the nucleus. For a few objects we are not able to measure meaningful values for all of the quantities and these are left blank in the table.

In Figures 1-4 we plot various relations between the observed and derived parameters described above. In Table 2 we give the derived correlation coefficients corresponding to plots shown in Figures 1 - 4.

Notes to Table 1: Velocities are in units of km sec $^{-1}$, radio power is in units of erg sec $^{-1}$ Hz $^{-1}$, emission-line luminosities are in units of erg sec $^{-1}$, all length scales are in kpc, M_{gass} and M_{dyn} are in solar mass units. Luminosities and masses are shown as logarithms.

references: 1) Baum, Heckman & van Breugel (1990); 2) McCarthy, Baum, & Spinrad (1995).

4. Correlation Results

Below we describe the most relevant correlation results.

Table 1. Data Table

Source 1	FR 2	PA 3	z 4	P ₄₀₈ 5	V _{peak} 6	V _{max} 7	D _[OII] 8	R _{Vmax} 9	L _[OII] 10	FWHM 11	D _{Rad} 12	l _{Rad} 13	M _{gas} 14	M _{dyn} 15	Ref 16
3CR 272.1	I	085	0.003	23.7	250	125	2	0.6	39.1	150 \pm 050	14	14	4.6	9.3	1
3CR 274.0	I	000	0.004	25.6	370	250	21	0.8	40.2	219 \pm 100	52	52	6.7	...	1
3CR 264.0	I	085	0.021	25.4	17	8.5	4	0.3	39.8	450 \pm 150	29	15	4.2	6.7	1
3CR 442.0	I	126	0.026	25.6	140	70	7	2	40.2	300 \pm 100	385	192	5.8	9.3	1
3CR 078.0	I	120	0.029	25.7	30	15	7	1.6	40.4	480 \pm 050	141	71	5.7	7.9	1
3CR 088.0	I	150	0.030	25.6	60	40	8	3	40.5	350 \pm 100	189	95	6.1	9.0	1
3CR 353.0	I	160	0.030	26.7	100	100	6	2	40.2	400 \pm 200	223	112	5.8	9.7	1
3CR 098.0	I	163	0.031	26.0	310	210	23	8	40.6	250 \pm 050	264	133	6.9	10.9	1
PKS 0634	II	124	0.056	26.5	480	260	60	14	42.2	150 \pm 100	1169	117	0.0	11.3	1
3CR 405.0	II	160	0.056	26.5	105	62	13	3	41.9	350 \pm 050	187	94	6.5	9.4	1
3CR 403.0	II	020	0.059	26.4	480	260	16	6	40.7	200 \pm 100	333	167	6.7	11.0	1
3CR 033.0	II	019	0.059	26.7	310	220	17	4	41.4	300 \pm 150	419	211	6.6	10.6	1
3CR 192.0	II	145	0.060	26.3	340	230	39	20	41.1	150 \pm 100	305	191	7.8	11.4	1
3CR 285.0	II	140	0.079	26.2	390	260	21	5	41.2	200 \pm 100	374	187	6.7	10.9	1
3CR 227.0	II	121	0.086	26.7	260	160	144	20	42.0	250 \pm 100	501	274	8.0	11.1	1
3CR 433.0	II	129	0.102	27.1	410	410	31	8	40.6	500 \pm 200	161	82	6.9	11.5	1,2
PKS 0745	I	112	0.103	26.7	75	75	34	7	42.5	355 \pm 100	31	16	8.0	...	1
PKS 1345	0	060	0.122	26.8	165	165	26	6	42.2	550 \pm 200	0.3	0.3	7.1	10.5	1
3CR 381.0	II	155	0.161	27.0	480	280	127	29	42.3	200 \pm 200	257	130	8.3	11.7	2
3CR 063.0	II	090	0.175	27.2	290	280	63	10	41.9	500 \pm 100	88	44	7.4	11.2	1
3CR 033.1	II	054	0.181	27.1	150	100	58	16	41.8	300 \pm 200	884	327	7.7	10.6	2
3CR 196.1	I	052	0.198	27.2	50	50	25	7.0	41.5	400 \pm 100	17	17	7.0	9.6	1
3CR 079.0	II	322	0.256	27.6	530	350	117	53	42.4	200 \pm 200	454	195	8.8	12.2	2
3CR 460.0	II	215	0.268	27.1	220	120	38	16	41.6	500 \pm 250	32	8	7.7	10.7	2
3CR 300.0	II	000	0.270	27.6	450	380	72	54	42.7	300 \pm 100	526	164	8.9	12.2	2
3CR 458.0	II	040	0.290	27.5	280	180	232	68	42.4	325 \pm 100	1099	633	9.0	11.7	2
3CR 458.0	II	040	0.290	27.5	350	300	232	68	42.4	350 \pm 150	1099	633	9.0	...	2
3CR 299.0	II	000	0.367	27.7	320	320	88	39	42.5	600 \pm 100	78	20	8.6	11.9	2
3CR 306.1	II	180	0.441	27.9	080	060	51	15	42.7	400 \pm 200	690	350	7.9	10.1	2
3CR 435.0	II	229	0.471	27.8	250	150	281	76	42.7	300 \pm 100	94	94	9.1	11.6	2
3CR 330.0	II	230	0.550	28.5	650	450	85	82	43.5	450 \pm 200	517	259	9.4	12.6	2
3CR 169.1	II	126	0.633	27.9	1500	1400	73	61	43.0	500 \pm 100	339	178	9.1	13.4	2
3CR 337.0	II	090	0.635	28.2	320	260	105	132	41.9	400 \pm 200	384	161	9.4	12.3	2
3CR 034.0	II	000	0.689	28.3	150	150	170	28	43.9	...	425	425	8.7	11.1	2
3CR 441.0	II	144	0.707	28.4	1100	1050	162	138	42.7	100 \pm 100	308	112	9.6	13.5	2
3CR 277.2	II	055	0.766	28.4	950	950	316	131	43.5	500 \pm 100	521	193	9.8	13.4	2
3CR 340.0	II	090	0.775	28.4	110	060	38	19	42.9	450 \pm 100	436	223	8.1	10.2	2
3CR 352.0	II	150	0.806	28.5	650	350	60	58	43.3	850 \pm 100	100	100	9.1	12.2	2
3CR 265.0	II	115	0.811	28.7	680	450	283	105	44.1	500 \pm 100	768	768	9.8	12.7	2
3CR 265.0	II	115	0.811	28.7	500	500	283	105	44.1	500 \pm 100	768	768	9.8	12.8	2
3CR 280.0	II	090	0.998	29.0	550	500	98	72	44.0	700 \pm 100	135	68	9.4	12.6	2
3CR 356.0	II	148	1.079	28.8	1500	1500	85	73	43.9	700 \pm 100	302	302	9.4	13.6	2
3CR 368.0	II	065	1.132	28.9	575	550	91	43	44.1	1400 \pm 100	93	93	9.0	12.4	2
3CR 267.0	II	090	1.140	28.9	380	380	31	21	43.3	750 \pm 250	416	192	8.3	11.8	2
3CR 324.0	II	090	1.206	29.0	725	500	92	53	44.0	1000 \pm 200	107	107	9.2	12.5	2
3CR 266.0	II	180	1.275	29.0	550	450	47	33	43.9	900 \pm 200	45	45	8.8	12.2	2
3CR 266.0	II	180	1.275	29.0	1350	1350	47	0.1	43.9	...	45	45	0.0	...	2
3CR 294.0	II	180	1.786	29.4	1300	1200	152	91	44.4	1100 \pm 200	173	77	9.7	13.4	2
MRC 0457	II	065	1.960	28.9	600	550	114	67	44.4	1400 \pm 300	200	96	9.5	12.6	2
MRC 0406	II	128	2.44	29.8	1900	1000	76	45	44.5	1000 \pm 300	89	55	9.2	14.0	2
MRC 2104	II	021	2.49	29.6	490	350	139	23	44.4	800 \pm 200	269	134	8.6	11.8	2

4.1. Radio Power with Redshift

In our sample, as in most flux limited samples extending to significant redshifts, radio power and redshift are strongly correlated making the disentanglement of redshift versus radio power effects a difficult challenge.

4.2. Log Gas Mass versus log Redshift

There is an apparent correlation of the ionized gas mass with redshift, with ionized gas mass increasing roughly linearly (in a log-log plot) with redshift (Figure 1a). Further, the plot shows that the FR1 and FR2 sources follow the same correlation. If this correlation is real (and not just a selection effect - see below), then there are two straightforward possible explanations for it.

- The mass of cold gas within the parent galaxies increases with redshift, such that cold gas was more abundant in radio galaxy hosts at earlier epochs. This is consistent with (1) increased bending in radio sources at high redshift (e.g., Barthel & Miley 1988); (2) the higher fraction of compact GHz Peaked Spectrum quasars at high redshift (e.g., O’Dea 1998); (3) the alignment effect occurring preferentially at high redshift (e.g., McCarthy 1993).
- The flux of ionizing radiation, and hence the measured mass of ionized gas for radiation bounded nebulae, increases with radio power (redshift).

However, some caution is needed in interpreting the data, as the correlation may owe at least in part, to an observational selection effect, since sources with small masses of ionized gas at high redshift would not have been detected as extended emission line sources and so would not have been included in follow up spectroscopic studies such as this one. That is, the limiting surface brightness curve defines an excluded region of the plot. However, despite this caveat, the sources in our sample do nevertheless show an order of magnitude or more variation in observed gas mass such that at low redshifts, (or radio powers) we do not find sources with as high gas masses as we do at higher redshift (power).

4.3. Dynamical Mass versus z

We also find an apparent correlation of redshift (and radio power) and enclosed dynamical mass (Figure 1b). FR1s have systematically low dynamical masses at a given redshift, and we find that the highest dynamical mass objects are double kinematic systems (see the correlation of redshift with V_{max} below), which are found preferentially at the highest z . The maximum derived dynamical masses are comparable to the masses of clusters, as derived from x-ray and lensing studies (Squires *et al.* 1997; Allen, Fabian, & Kneib 1996; Miralda-Escudé & Babul (1995)), at comparable distances from the cluster center (e.g., 100 kpc). There are two ways to understand this correlation, assuming for the moment that the velocities do measure the gravitational potential and not the radio source jet thrust.

- The mass of the host galaxy is larger at redshifts and radio powers. This seems somewhat unlikely given that radio galaxies live in the most massive galaxies even at low redshifts, and that it is well known (Ledlow & Owen 1996; de Vries *et al* 1998) that at present FR1s (and not FR2s) on average occupy higher mass systems at a fix radio luminosity.
- The ionized gas probes progressively larger scales at higher redshift, thereby enclosing greater and greater dynamical mass. This could be due either to the presence of more cold gas in the host galaxies at higher z (see above) or, to the increased UV ionizing flux put out by the more powerful radio galaxies at high redshift in our sample.

4.4. Dynamical mass versus M_{gas}

There is a strong apparent correlation of inferred dynamical mass with gas mass, with a slope near one half - that is dynamical mass proportional to the square root of the gas mass (Figure 2a). The correlation for FR1 and FR2 radio galaxies is the same, with the FR1s occupying the low mass portion of the relationship.

If the correlation is real (and the inferred dynamical mass is really a measure of enclosed mass) it suggests that

- there is a constant fraction of gas to gravitational mass of $\sim 0.1\%$ and
- the ionized gas mass measures gas mass and not ionizing flux.

We tested for the possibility that this correlation is artificial, since one of the quantities depends on R and the other on R^3 by plotting $R \times V$ against the [OII] luminosity directly; the correlation, though noisier, remains (see Figure 2c).

4.5. V_{max} vs. $R_{V_{max}}$

There is an apparent correlation of maximum velocity versus the radius in kpc at which that maximum velocity is measured, with a slope near unity, such that the larger the distance, the larger the velocity (Figure 2d). FR1s fit on the same relationship as FR2s. This can be most simply interpreted in the following way. The velocities are gravitationally induced, all radio galaxies have basically the same intrinsic masses and environments, and the further out one probes the gas velocity, the greater the velocity one measures since a larger mass is encircled. In the most powerful radio sources (or the highest redshift sources) - the larger luminosity or ionizing radiation (which is assumed to scale with radio luminosity) illuminates gas at larger radii from the galaxy nucleus, producing this result.

Interestingly, we see from this plot that the maximum velocity which is measured is roughly 1500 km sec^{-1} . What can this mean? Two alternate scenarios present themselves;

- If the velocities are gravitational in origin, than as mentioned above, 1500 km sec^{-1} is roughly the velocity predicted for gas in equilibrium within a very rich cluster at a distance of $\sim 100 \text{ kpc}$ from the nucleus (e.g., Mazure *et al.* 1996). It appears, however, that many of the $v > 800 \text{ km sec}^{-1}$ systems are composites (i.e., two galaxies); the maximum velocity would then be a measure of the peak galaxy encounter velocity. Again, 1500 km sec^{-1} is a sensible pair-wise encounter velocity. It is interesting to consider whether pairs can produce such velocities without obvious clusters at redshifts of $0.6 - 0.7$ (e.g. 3C 169.1, 3C 277.2 where these high velocities are also seen). We return to this later in the discussion.
- If the velocities are shock induced from the radio source and not gravitational, then the maximum of 1500 km sec^{-1} may correspond to the maximum velocity achieved before the gas is heated to temperatures such that the radiative cooling time is longer than the source lifetime. Bicknell, Dopita and O'Dea (1997) assert that detailed fast radiative shock models fit the following relationship: $t_{rad,6} \sim 1.9n^{-1}V_3^{2.9}$ where V_3 is the shock velocity in units of 1000 km/sec , n is the preshock density. Thus for $V = 1500 \text{ km/sec}$ and a radio lifetime = 10^7 years , only clouds with densities greater than 0.6 cm^{-3} will produce significant optical and near-UV line emission. At higher shock velocities or lower preshock densities the heated gas will be too hot and diffuse to cool within the radio source lifetime.

4.6. FWHM and V_{max} versus $l_{\text{Rad}}/R_{V_{max}}$

The plots of FWHM and V_{max} versus $l_{\text{Rad}}/R_{V_{max}}$ (Figures 4a and 4b) are helpful in disentangling the relationship between the radio source and the observed velocities; if the radio source is responsible for inducing the turbulence in the gas then we might expect that there would be a strong correlation between the FWHM (or V_{max}) and the ratio of radio source to emission line nebulae size. That is, we might expect that when the radio source and the nebulae are comparably sized, the gas will be most kinematically disturbed.

There appears to be a weak correlation with a trend towards larger line widths in objects with comparable radio and emission-line sizes. However, this is not a statistically robust correlation and there is a large ranges in FWHM and V_{max} values for a given relative size. Interestingly, the FR1s follow the same correlation as the FR2s. Longair et al. (1999) report a significant correlation between source size and off-nuclear line widths in a small sample of $z \sim 1$ 3CR galaxies.

4.7. FWHM versus z

There is an apparent correlation of line width and redshift (and radio power), which warrants further examination. The plot of FWHM versus z (Figure 3a) is essentially flat for $0.01 < z < 0.6$ and rises steeply (or jumps) for larger redshifts. The highest line widths are seen at $z > 1$; for $z < 1$ the maximum line width is 500 km sec^{-1} and the mean is $370 \pm 150 \text{ km sec}^{-1}$ while for $z > 1$, the maximum is 1500 km sec^{-1} and the mean is $1000 \pm 250 \text{ km sec}^{-1}$. The FR1 sources have relatively high mean line widths relative to FR2 sources at the same redshift with an FR1 mean of $\sim 385 \pm 95 \text{ km sec}^{-1}$ and an FR2 mean of $\sim 285 \pm 130 \text{ km sec}^{-1}$ at $z < 0.2$.

The change in properties at redshifts above $z \sim 0.6$ could signal a difference in environments of the host galaxies. At low redshift FR2s are predominantly found in the field or groups of galaxies (e.g., Prestage & Peacock 1988), while at higher redshifts they are believed to be found in environments with densities reaching those of rich clusters (e.g., Hill & Lilly 1991). Thus, if the line width reflects the underlying gravitational potential, the observed FWHM may trace the velocity dispersion of the host galaxy or its surrounding group or cluster. The systematically high FWHM of FR1 sources relative to FR2 sources at low redshifts is grossly consistent with this scenario, since FR1s occupy more massive galaxies at a given radio luminosity and inhabit denser environments at low redshifts than do FR2s (Ledlow & Owen 1996; Hill & Lilly 1991).

In the alternative scenario, where the FWHM reflects an interaction with the radio source, this same plot can be interpreted as FWHM versus radio power. At higher powers

the interaction is stronger and the turbulence induced in the gas greater. It is not clear how this scenario would produce the sudden change in line widths at $z > 0.6$.

4.8. V_{max} versus z

The V_{max} versus z plot is similar to the FWHM versus z plot and could reflect the same process involved in the change in line widths at large redshifts. Specifically, if one excludes the FR1s, which have systematically low velocities at a given redshift (see the subsection 4.9 below for an explanation of the FR1 behavior) then the velocities are flat for $0.01 < z < 0.7$ at a mean of $\sim 230 \pm 240$ km sec $^{-1}$ and then the mean value jumps dramatically to $v \sim 720 \pm 400$ km sec $^{-1}$ for $z > 1$. This is, again, most likely due to a change in environments of the host galaxies, but may also reflect the importance of radio power in determining the overall gas kinematics. In the latter scenario, it is, however, difficult to understand why one would see a ‘jump’ at intermediate redshifts as opposed to a continuous correlation of velocity with radio power.

Special consideration should be given to the highest V_{max} systems. We note that of the sources with V_{max} greater than ~ 800 km sec $^{-1}$ approximately six of these sources show double kinematic structure. 3C 169.1, 3C 356 and MRC 2104-242 for example, are systems with two fully detached emission line regions with velocity differences of several hundred km sec $^{-1}$ or more (see McCarthy, Baum, & Spinrad (1996) for velocity versus distance plots). These are likely to be instances where we are seeing gas in two distinct kinematic systems, for example two independent galaxies, or gas in “split-line” systems where the gas has been wrapped around two sides of expanding radio plasma interacting with out-flowing radio plasma (e.g. Clark et al. 1997; Capetti et al. 1999) We also note that the maximum values of V_{max} seen are roughly $\sim 1200 - 1500$ km sec $^{-1}$. See also the discussion under 4.5 above.

4.9. FWHM/ V_{max} versus P_{408}

The FR1 sources cleanly separate from the FR2 sources on this plot of FWHM/ V_{max} versus P_{408} (Figure 3d). In the mean the FR1s have appreciably higher ratios of FWHM to maximum velocity than the FR2s (8:2) at the same radio power. As Figures 3c and 3d show, FR1s have both larger line widths and lower maximum velocities at a given redshift than do the FR2s. This is consistent with the earlier results from Baum *et al.* (1992) that

indicated that the emission line gas in FR1 sources was dominated by turbulent motions, while that in FR2s showed a stronger component of systematic motions (e.g., rotation, outflow, or inflow). This plot also shows that the ratio of turbulent to systematic motion shows no evolution with radio power or redshift for the FR2s. This seems to suggest a common origin for both the turbulent and the systematic motions seen in the gas.

5. Discussion

As is typically the case for flux limited samples, radio power and redshift are very tightly coupled in our sample, making the deconvolution of radio power and redshift affects difficult, at best. A crucial question we must, nevertheless, seek to address is whether the kinematics we observe are due primarily to interactions between the gas and the outflow from the central engine or whether they reflect the underlying potential of the host galaxy. A similar question was addressed before for the emission line gas in Seyfert galaxies (Whittle 1992) and in nearby FR1 and FR2 radio galaxies (Baum *et al.* 1992). In both cases the conclusion was that the bulk of the velocities observed were dictated by the underlying gravitational potential and not by jet-gas interactions, though in both cases examples where that rule was violated and jet-gas interactions were dominant, were noted. In the high redshift/high radio power sample we address in this paper where we expect the outflow to be stronger and the gas environment to be richer, we might expect jet-gas interactions to be more dominant. Looking at the statistical data as a whole, however we find no evidence which *requires* jet interaction as the source of the gas kinematics. As is the case for their nearer by AGN brethren, the emission line kinematics even in the bulk of these high redshift/high power sources can be explained by gravity and not interaction, though as described below if the kinematics are gravitational in origin, the highest velocities seen point to interesting environments for intermediate and high redshift radio galaxies.

The apparent correlations of radio power with gas FWHM, Vpeak and $R_{V\max}$ point towards the importance of jet-gas interactions. However, it is not possible to distinguish with our sample, whether these correlations are primarily with redshift rather than radio power. Further, additional correlations with radio power or source size might have been expected if jet-gas interactions dominate the kinematics of the gas. For instance, if jet-gas interactions are dominant, one might have naively expected that either smaller radio sources, i.e., those which are trapped within the ISM of the host galaxy, or sources in which the radio source and emission line nebulae were of localized on the same size scales would evidence stronger jet-gas interactions. However, no correlations are seen between

the size of the radio source and the FWHM or maximum velocity of the gas. Similarly, no substantial correlation is seen between the FWHM or the maximum velocity of the radio source and the ratio of the radio to nebular size. Lastly, our sample shows no correlation of radio size with radio power or redshift, or of radio size with nebular size, but does show a substantial correlation of nebular size with redshift and/or radio power. Taken as a whole these findings would seem to indicate that the properties of the emission line nebula are coupled with redshift or radio power but not with the properties of the radio source.

Thus, the kinematics and correlations we see, can *most easily* (though not necessarily correctly of course) be interpreted in terms of a gravitational origin for the kinematic properties of the gas. To wit; we find that the FWHM, maximum velocity, radius at which maximum velocity is seen, apparent dynamic mass and gas mass all correlate with redshift (or radio power). In addition, we find that the maximum velocity and radius of maximum velocity are themselves correlated, as are the inferred dynamical mass and the gas mass, and the maximum velocity and gas mass. A plausible scenario which encapsulates the observations follows.

- The emission line nebulae are largely ionization (and not matter) bounded. That is, there is an abundance of cold gas in the ISM of the radio galaxies and when there is more ionizing radiation, more of the cold gas, and to further distances in the ISM, is illuminated and heated.
- The UV ionizing flux of the central engine is correlated with radio power (hence redshift in our sample) such that at higher power (redshift) there is a higher UV ionizing flux and hence emission line gas is found to greater radii.
- The emission line gas kinematics (both the line widths and the absolute velocities) are dominated by gravitational effects and therefore reflect the underlying potential at the distance where the gas is found.

If we take this model at face value, for the moment, we can then use it to understand the nature of the environments of powerful radio galaxies as a function of redshift. Specifically, at high redshift, where the highest rotational velocities are seen, we would have to be seeing the gravitational potential of not only the radio galaxies, but a cluster or group which surrounded it. The velocity separations seen ($1200\text{-}1500\text{ km sec}^{-1}$) approach those of the richest clusters seen at lower redshift (e.g., Mazure *et al.* 1996). This either indicates that high redshift high power radio galaxies are uniquely situated in the deepest potentials or it suggests that the host galaxies of powerful radio galaxies at high redshift are in pre-virialized environments in which infall may still dominate the kinematics.

Completely alternative models in which the kinematics are dominated by interactions with the radio source cannot be ruled out. Detailed studies show that such interactions are clearly occurring in some sources and so must play at least a part in determining some of the kinematics we see. For instance, an alternative interpretation of the sources which exhibit two very high velocity emission systems is that we are observing split line systems created by interactions of the cocoon of the expanding radio source with cold gas in the galaxy atmosphere, such as appears to be the case in the low velocity systems studied in detail such as Cygnus-A (3C405; Tadhunter et al. 1999) and 3C171 (Clark et al. 1998). If the velocities are shock induced from the radio source and not gravitational, then the maximum of 1500 km sec^{-1} must correspond to the maximum velocity achievable without heating the gas to temperatures so hot that the radiative cooling time is greater than the lifetime of the radio source. Applying the models of Bicknell, Dopita, and O’Dea (1998), this would constrain the pre-shock particle densities of the shocked clouds we see to be $n_e > 0.6 \text{ cm}^{-3}$.

6. Summary

We report the results of a study of the kinematics and morphology of the emission line nebula in powerful 3CR radio galaxies from redshift \sim zero to ~ 4 based on the data presented in Baum, Heckman and van Breugel (1990) and McCarthy, Baum, and Spinrad (1996) and additional data gathered on these and similar sources from the more general literature. The 3CR is a well-defined radio-flux limited sample; radio power (AGN luminosity) is strongly correlated with redshift in this sample.

We investigate the correlation of the kinematic properties of the gas with other inherent properties, such as redshift, radio and line luminosity, radio and emission line morphology and extent. We also investigate correlations with derived properties such as inferred mass of emission line gas and apparent dynamical mass, where the apparent dynamical mass is defined to be the mass required to gravitationally induce the observed kinematics. We find that both the inferred mass in emission line gas and the apparent dynamical mass appear to increase with redshift (or radio power).

For each source we define a maximum emission line velocity (V_{\max} , the maximum difference between gas velocity and the systemic velocity of the galaxy, measured as the emission line velocity at the continuum peak) and the projected radius at which that maximum velocity occurs ($R_{V_{\max}}$). We find that across the full sample, the maximum emission line velocity increases with $R_{V_{\max}}$ and with the absolute size of the nebula. We

also find that the sources with the highest maximum velocities (1000-1500 km sec⁻¹) are those with two independent kinematic systems present.

No correlations are seen between the size of the radio source and the FWHM or maximum velocity of the gas. Similar to the above, no substantial correlation is seen between the FWHM or the maximum velocity of the radio source and the ratio of the radio to nebular size. Lastly, our sample shows no correlation of radio size with radio power or redshift, or of radio size with nebular size, but does show a substantial correlation of nebular size with redshift and/or radio power.

These results are consistent with (but do not necessitate) a picture in which the kinematics of the emission line gas are predominantly dictated by gravity and the line luminosity of the nebula is predominantly determined by the ionizing luminosity of the central engine. If the mass of cold gas increases with redshift, then the increasingly powerful AGN present in the 3CR sample at higher redshift, will illuminate a larger ionized nebula. If the velocities are predominantly gravitational, then the most powerful sources which are at the highest redshifts in our sample, and show the highest emission line gas velocity, would have to be found in very deep gravitational potentials, such as cluster environments. Alternatively, at the highest redshifts, powerful radio galaxies may be in environments which are in a relatively young evolutionary state where the kinematics are still dominated by infall. In the gravitational interpretation, the very highest velocity systems, with apparently disjoint multiple velocity systems in the nebula of a given source, are cases where two galaxies are merging or interacting, and gas systems associated with each galaxy are seen.

7. Acknowledgments

We thank the staffs of the Kitt Peak and Cerro Tololo sites of the National Optical Astronomy Observatories as well as those of the Lick and Palomar Observatories. At the time these observations were being carried out, the Carnegie Institution had access to the Hale 5m telescope under a cooperative agreement with the California Institute of Technology.

Fits to Correlations	
Relationship	Correlation Coefficient
(1)	(2)
P_{408} vs z	0.98
$R_{V\max}$ vs z	0.82
M_{gas} vs z	0.77
$R_{V\max}$ vs V_{\max}	0.76
V_{\max} vs M_{gas}	0.76
M_{dyn} vs z	0.75
P_{408} vs V_{\max}	0.67
V_{\max} vs z	0.64
M_{gas} vs M_{dyn}	0.64
P_{408} vs FWHM	0.63
FWHM vs z	0.62
$l_{\text{Rad}}/R_{V\max}$ vs V_{\max}	0.43*
$l_{\text{Rad}}/R_{V\max}$ vs FWHM	0.41*
D_{Rad} vs $D_{[\text{OII}]}$	0.34
FWHM vs M_{gas}	0.32
D_{rad} vs FWHM	0.26*
D_{rad} vs V_{\max}	0.26
V_{\max} vs FWHM	0.20
D_{rad} vs z	0.10

Table 2: The results of a least squares linear fit to the relationships in log-log space. Uncertainties are in parentheses.

REFERENCES

- Allen, S. W., Fabian, A. C., Kneib, J. P., 1996, MNRAS, 279, 616
- Barthel, P. D., & Miley, G. K., 1988, Nature, 333, 319
- Baum, S. A., Heckman, T., Bridle, A., van Breugel, W., & Miley, G. 1988, ApJS, 68, 643
- Baum, S. A., & Heckman, T. 1989a, ApJ, 336, 681
- Baum, S. A., & Heckman, T. 1989b, ApJ, 336, 702.
- Baum, S. A., Heckman, T., & van Breugel, W. 1992, ApJ, 389, 208
- Baum, S. A., Heckman, T., & van Breugel, W. 1990, ApJS, 74, 389
- Baum, S. A., Zirbel, E. L., & O'Dea, C. P., 1995, ApJ, 451, 88
- Best, P., Longair, M., & Rottgering, H. 1999, in "The Hy-Redshift Universe", ASP Conf. Series, A. Bunker & W. van Breugel, eds. in press
- Bennet, A. S. 1962, MNRAS, 68, 163
- Bicknell, G. & Koekemoer, A. 1995, in IAU Symp 175, "Extragalactic Radio Jets", R. Ekers et al. eds., p 473.
- Bicknell, G., Dopita, M. A., & O'Dea, C. P., 1997, ApJ, 485, 112
- Capetti, A., Axon, D., Macchetto, F. D., Marconi, A. Winge, C. 1999, ApJ, 516, 187
- Clark, N. E., Axon, D. J., Tadhunter, C. N., Robinson, A., O'Brien, P. 1998, ApJ, 494, 546
- Djorgovski, S., Spinrad, H., McCarthy P., Dickinson, M., van Breugel, W., & Strom, R. 1988, AJ, 96, 836
- Ellingson, E., Green, R., & Yee, H. 1991, ApJ 371, 49
- Fanaroff, B., Riley, J. M. 1974, MNRAS, 167, 31
- Gelderman, R. & Whittle, M. 1994, ApJS, 91, 491
- Heckman, T. M., Baum, S. A., van Breugel, W. J. M., & McCarthy, P. 1989, ApJ, 338, 48
- Hill, G. J., & Lilly, S. J., 1991, ApJ, 367, 1

- Ledlow, M. J., & Owen, F. N., 1996, AJ, 112, 9
- Leahy, J. P., Bridle, A., & Strom, R. G. 1995, in "Extragalactic Radio Sources", R. D. Ekers et al., eds., Kluwer, IAU Symp. 175, 157
- Longair, M., et al. 1999, in "The Hy-Redshift Universe", ASP conference series, in press.
- Mazure, A. *et al.* 1996, A&A, 310, 31
- McCarthy, P. 1993, Ann. Rev. A&Ap, 31, 639
- McCarthy, P. J., van Breugel, W. J. M., Spinrad, H., & Djorgovski, S. 1987, ApJ, 321, L29
- McCarthy, P., van Breugel, W., & Kapahi, V. 1991, ApJ, 371, 478
- McCarthy, P., Spinrad, H., & van Breugel, W., 1995, ApJS, 99, 27
- McCarthy, P. J., Baum, S. A., & Spinrad, H. 1996a, ApJS, 106, 281
- McCarthy, P. J., Kapahi, V. K., van Breugel, W., Persson, S. E., Athreya, R., & Subrahmanya, C. R., 1996b, ApJS, 107, 19
- Miley, G. K., Chambers, K. C., van Breugel, W., Macchetto, F. 1992, ApJ, 401, L69
- Miralde-Escudè, J., & Babul, A., 1995, ApJ, 449, 18
- O'Dea, C. P., 1998, PASP, 110, 493
- Prestage, R. M., Peacock, J. A. 1988, MNRAS, 230, 131
- Rawlings, S. & Saunders, R. 1991, Nature, 349, 138
- Robinson, A., Binette, L., Fosbury, R. A. E., Tadhunter, C. N. 1987, MNRAS, 227, 97
- Spinrad, H., Djorgovski, S., Marr, J., & Aguilar L. A. 1985, PASP, 97, 932
- Squires, G., Neumann, D. M., Kaiser, N., Arnaud, M., Babul, A., Boehringer, H., Fahlman, G., & Woods, D., 1997, ApJ, 482, 648
- Strom, R. G., Riley, J. M., Spinrad, H., van Breugel, W., Djorgovski, S., Liebert, J., & McCarthy, P. 1990, A&A, 227, 19
- Tadhunter, C. N., Fosbury, R. A. E., & Quinn, P. J., 1989, MNRAS, 240, 225
- Tadhunter, C. N., Packham, C., Axon, D. J., Jackson, N. J., Hough, J. H., Robinson, A., Young, S., Sparks, W. 1999 MNRAS, 307, 24

- Tadhunter, C. N., Morganti, R., Robinson, A., Dickson, R., Villar-Martin, M., & Fosbury, R. A. E. 1999, 298, 1035
- Villar-Martin, M., Tadhunter, C. N., Clark, N., 1997, A&A, 323, 21
- Villar-Martin, M., Tadhunter, C. N., Morganti, R., Clark, N., Killeen, N., & Axon, D. 1998, A&A, 332, 479
- Villar-Martin, M., Binette, L., & Fosbury, R. A. E. 1999, A&A, 346, 7
- de Vries, *et al.* 1997, ApJS, 110, 191
- de Vries, W. H., O'Dea, C. P., Baum, S. A., Perlman, E., Lehnert, M. D. & Barthel, P. D. 1998, ApJ 503, 156
- Whittle, M., 1992, ApJ, 387, 109
- Xu, C., Livio, M. & Baum, S., 1999, AJ, 118, 1169
- Yates, M., Miller, L., & Peacock, J. 1989, MNRAS, 240, 129

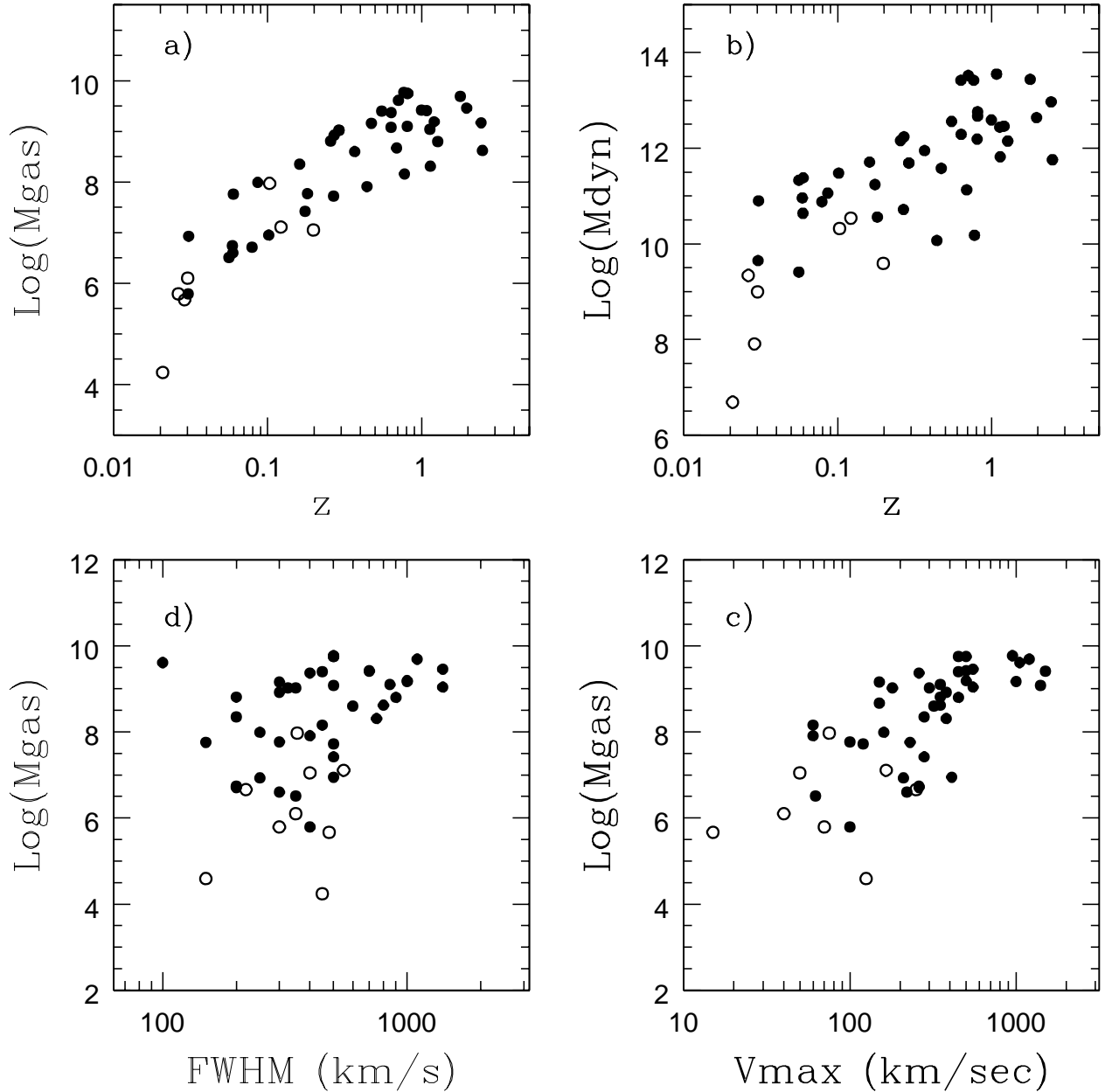


Fig. 1.— In each of the panels of this figure, and the three subsequent figures, the filled symbols refer to FRII sources, while the open symbols represent FRI and transition sources. In the upper panels the mass of ionized gas and the apparent dynamical mass are plotted against redshift. In the lower panels the derived mass of ionized gas is plotted against the maximum FWHM (left) and the maximum velocity (right). All of the masses are shown in units of M_{\odot} .

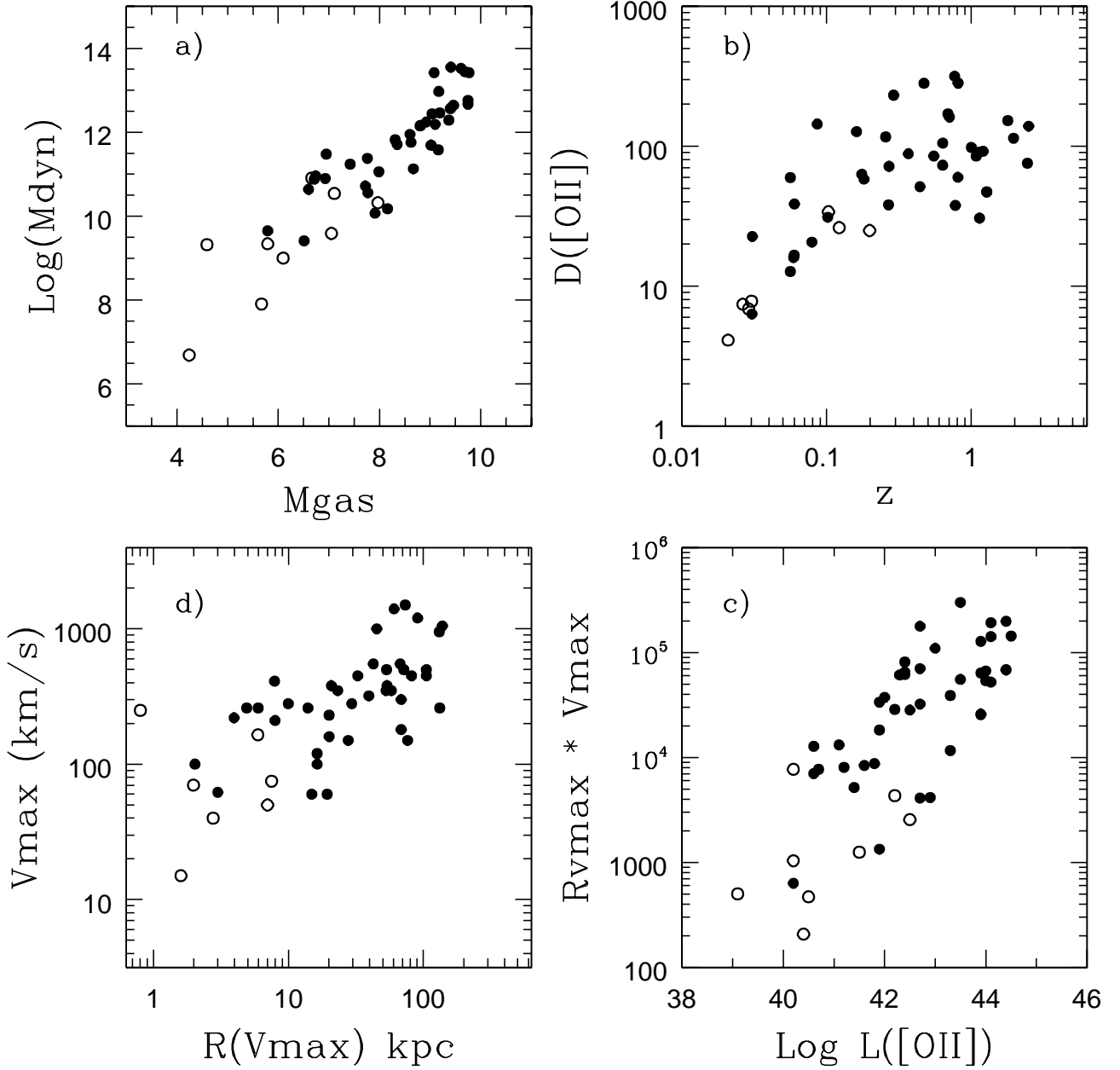


Fig. 2.— In the upper left the apparent dynamical mass is plotted against the derived mass of ionized gas. See the discussion in the text of the degeneracy between these derived quantities. The isophotal emission-line size is plotted against redshift in the upper right panel, while the maximum velocity is plotted against the radial position of the fastest moving [OII] emission in the lower left. The lower right panel shows the run of $R_{V_{\text{max}}} \times V_{\text{max}}$ with emission-line luminosity.

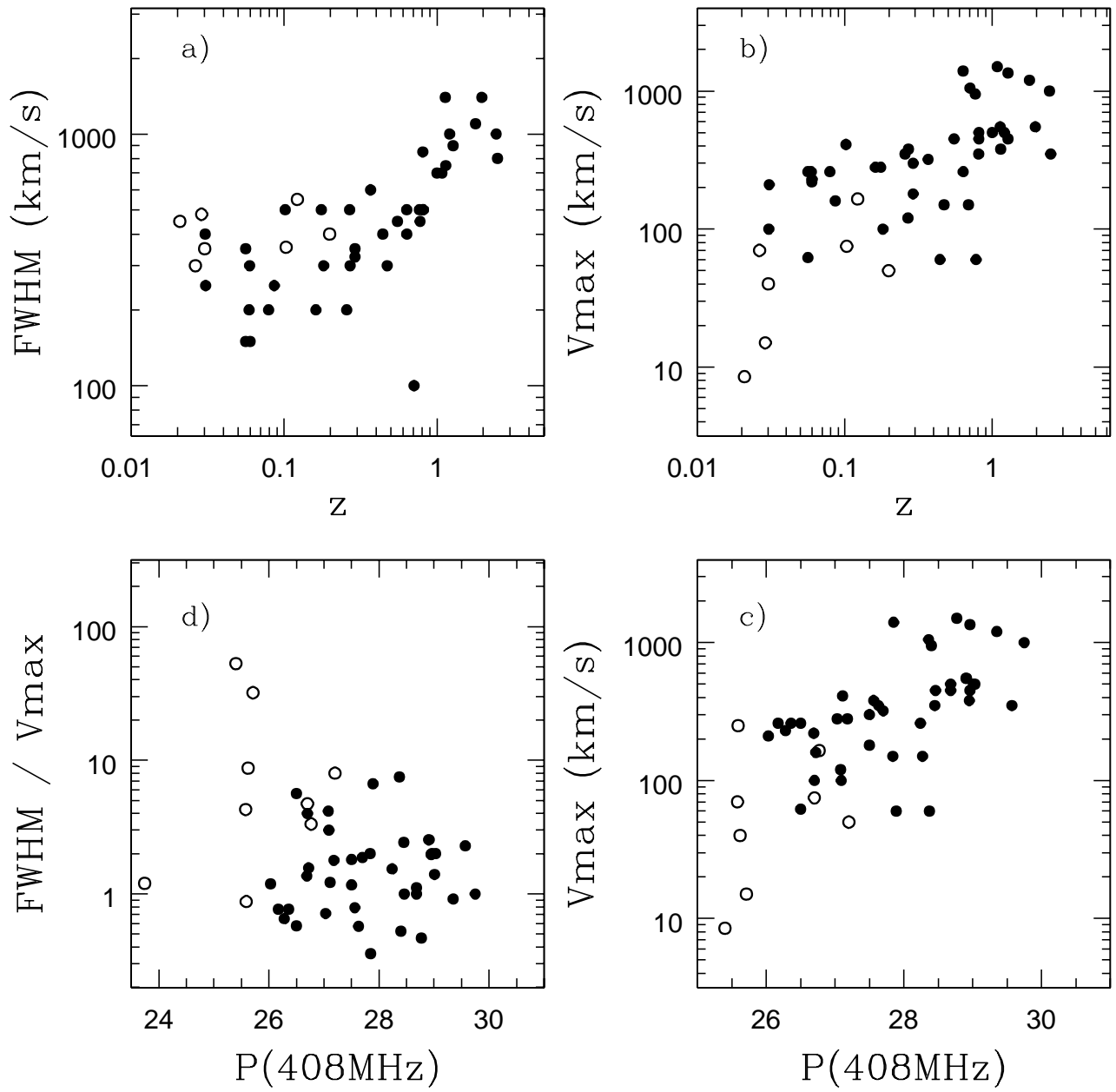


Fig. 3.— The upper left and right panels show the run of FWHM and V_{Max} against redshift, while the lower panels show the ratio of the FWHM to the maximum velocity (left) and maximum (right) velocity against the 408MHz monochromatic radio power.

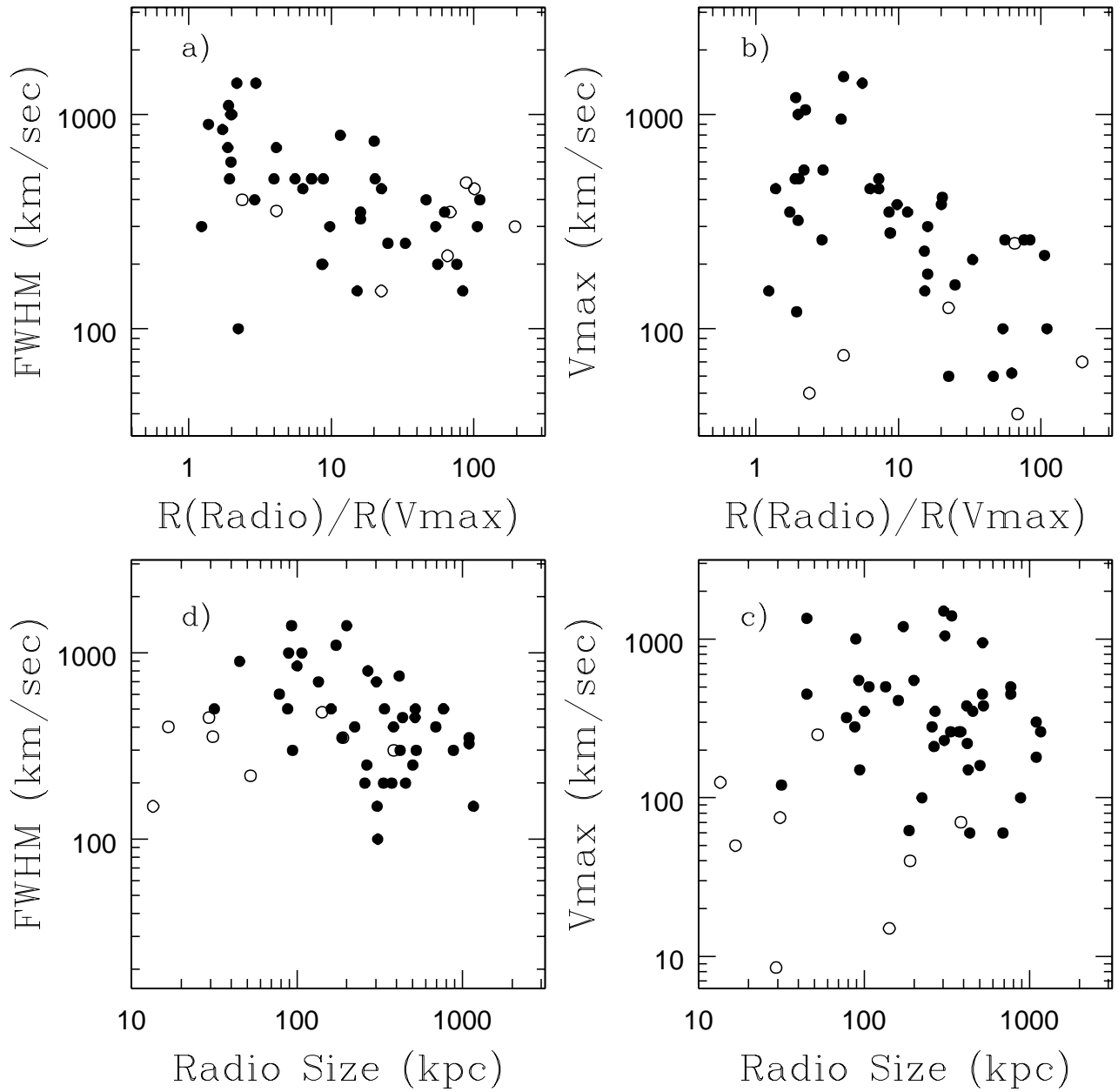


Fig. 4.— Plotted are the off-nuclear FWHM (upper left) and the maximum velocity (upper right) against the ratio of the radio and emission line sizes. The lower left and right panels show the same quantities plotted against the full linear size of the radio source.